Astronomy
&
Astrophysics

The first XMM-Newton slew survey catalogue: XMMSL1

R. D. Saxton[1], A. M. Read[2], P. Esquej[3,1], M. J. Freyberg[3], B. Altieri[1], and D. Bermejo[1,4]

[1] XMM SOC, ESAC, Apartado 78, 28691 Villanueva de la Cañada, Madrid, Spain
  e-mail: richard.saxton@sciops.esa.int
[2] Department of Physics and Astronomy, University of Leicester, Leicester LE1 7RH, UK
[3] Max-Planck-Institut für extraterrestrische Physik, 85748 Garching, Germany
[4] Instituto de Astrofisica de Andalucia, CSIC, Granada, Spain

ABSTRACT

Aims. We report on the production of a large area, shallow, sky survey, from XMM-*Newton* slews. The great collecting area of the mirrors coupled with the high quantum efficiency of the EPIC detectors have made XMM-*Newton* the most sensitive X-ray observatory flown to date. We use data taken with the EPIC-pn camera during slewing manoeuvres to perform an X-ray survey of the sky.
Methods. Data from 218 slews have been subdivided into small images and source searched. This has been done in three distinct energy bands; a soft (0.2–2 keV) band, a hard (2–12 keV) band and a total XMM-*Newton* band (0.2–12 keV). Detected sources, have been quality controlled to remove artifacts and a catalogue has been drawn from the remaining sources.
Results. A "full" catalogue, containing 4710 detections and a "clean" catalogue containing 2692 sources have been produced, from 14% of the sky. In the hard X-ray band (2–12 keV) 257 sources are detected in the clean catalogue to a flux limit of 4×10^{-12} ergs s^{-1} cm^{-2}. The flux limit for the soft (0.2–2 keV) band is 6×10^{-13} ergs s^{-1} cm^{-2} and for the total (0.2–12 keV) band is 1.2×10^{-12} ergs s^{-1} cm^{-2}. The source positions are shown to have an uncertainty of 8″ (1σ confidence).

Key words. X-rays: general – surveys – catalogs

1. Introduction

There is a strong tradition in X-ray astronomy of using data taken during slewing manoeuvres to perform shallow surveys of the sky. The Einstein (Elvis et al. 1992), Exosat (Reynolds et al. 1999) and RXTE (Revnivtsev et al. 2004) slew surveys all provide a useful complement to dedicated all-sky surveys such as ROSAT (Voges et al. 1999) and HEAO-1 (Piccinotti et al. 1982) and the smaller area, medium sensitivity ASCA survey (Ueda et al. 1999) and pencil-beam XMM-*Newton* (Hasinger et al. 2001) and Chandra (Brandt et al. 2000) deep looks. It was long recognised that XMM-Newton (Jansen et al. 2001) with its great collecting area, efficient CCDs, wide energy band and tight point-spread function (PSF) has the potential to make an important contribution to our knowledge of the local universe from its slew data. Early estimates (Lumb 1998; Jones & Lumb 1998), based on an expected slewing speed of 30 degrees per hour, and a slightly lower background level than that actually encountered in orbit, predicted a 0.5–2 keV flux limit of 2×10^{-13} erg cm^{-2} s^{-1}. While the chosen in-orbit slew speed of 90 degrees per hour reduces the sensitivity, initial assessments of the data showed that the quality of the data is good and that many sources are detected (Freyberg et al. 2005). A review of properties shows that the XMM-*Newton* slew survey compares favourably with other large area surveys in terms of depth and positional accuracy (Table 1).

During slews all the three imaging EPIC cameras take data in the observing mode set in the previous pointed observation and with the Medium filter in place. The slew speed of 90 degrees per hour combined with the slow readout time of the MOS detectors (2.6 s; Turner et al. 2001) means that sources appear as

Table 1. Properties of large area X-ray surveys.

Satellite	Energy range (keV)	Coverage[a] % of sky	Flux lim. [b]	Position error
RASS	0.2–2.4	92	0.03	12″
Einstein slew	0.2–3.5	50	0.3	1.2′
XMM slew (soft)	**0.2–2**	**14**	**0.06**	**8″**
EXOSAT slew	1–8	98	3	20′
HEAO-1/A2	2–10	100	3	60′
RXTE slew	3–20	95	1.8	60′
XMM slew (hard)	**2–12**	**14**	**0.4**	**8″**

[a] The XMM-*Newton* slew sky coverage has been computed by adding the area contained in all of the images used in source searching with an exposure time greater than 1 s.
[b] Flux limit, units of 10^{-11} ergs s^{-1} cm^{-2}.

long streaks in the MOS cameras but are well formed in the fast observing modes of the pn camera (Strüder et al. 2001). For this reason, only the EPIC-pn data have been analysed.

In this paper we present a catalogue drawn from slews taken between revolutions 314 and 978 covering a sky region of 6240 square degrees. The main properties of the slew survey discussed in this paper are given in Table 2.

Slews have been source searched down to a likelihood threshold of 8, which after manual rejection of false detections gives 4710 candidate sources. Using simulations we have been able to identify a subset of high significance sources, with a likelihood threshold dependent upon the background conditions, that gives 2692 sources with a spurious fraction of ~4% (the "clean" catalogue). Of these, 2621 are from unique sources. In the hard (2–12 keV) band the clean catalogue contains

Table 2. Properties of the XMM-*Newton* slew survey.

Property	Range (keV)		
	0.2–2	2–12	0.2–12
Observing time (s)	5.4×10^5	5.4×10^5	5.4×10^5
Mean exposure time[a]	6.2 s	6.0 s	6.1 s
Total number of photons	1.6×10^6	2.2×10^6	3.8×10^6
Mean background[b]	0.09	0.14	0.23
Median source count rate[c]	0.68	0.90	0.81
Limiting source flux[d]	6.0×10^{-13}	4.0×10^{-12}	1.2×10^{-12}
Num. sources (full cat)[e]	2606	692	3863
Num. sources (clean cat)[e]	1874	257	2364

[a] The mean exposure time, after correcting for the energy-dependent vignetting.
[b] cnts/arcmin^2.
[c] cnts/s.
[d] ergs/s/cm^2. Based on a detection of 4 photons from a source passing near the detector centre (exp. time = 10 s), with a power-law spectrum of slope 1.7 and galactic absorption of 3×10^{20} atoms cm^{-2}.
[e] The number of sources flagged as good in the full and clean catalogues (see text).

257 sources (253 unique) of which ∼9% are expected to be due to statistical fluctuations.

The slew catalogue and accompanying images and exposure maps have been made available through the XMM Science Archive (XSA) as a queryable database and as FITS files[1]. A summary of scientific highlights from the slew survey has been published in Read et al. (2006).

2. Data selection

The XMM-*Newton* satellite moves between targets by performing an open-loop slew along the roll and pitch axes and a closed-loop slew, where measurements from the star tracker are used in addition to the Sun-sensor measurements to provide a controlled slew about all three axes, to correct for residual errors in the long open-loop phase. The open-loop slew is performed at a steady rate of about 90 degrees per hour and it is data from this phase which may be used to give a uniform survey of the X-ray sky.

Slew Data Files (SDF) have been stored in the XSA from revolution 314 onwards (before this date slews were performed with the CLOSED filter in place and no scientifically useful data was taken). Data from revolutions 314 to 978 have been used for this first catalogue but slews continue to be accumulated and increments to the catalogue are planned to be released on a regular basis. Only science data from slews with a duration of greater than 30 min were downlinked during the majority of these revolutions[2]. For the *Slew Survey* catalogue we have selected only EPIC-pn exposures performed in *Full Frame* (FF), *Extended Full Frame* (eFF), and *Large Window* (LW) modes, i.e. modes where all 12 CCDs are integrating (in LW mode only half of each CCD). The corresponding cycle times are 73.36 ms, 199.19 ms, and 47.66 ms, which converts to a scanned distance of 6.6 arcsec, 17.9 arcsec, and 4.3 arcsec per cycle time, respectively for a slew speed of 90 degrees per hour. In the *Small Window* mode only the central CCD is operated and a window of 64×64 pixels is read out, i.e. only about 1/3 of the single,
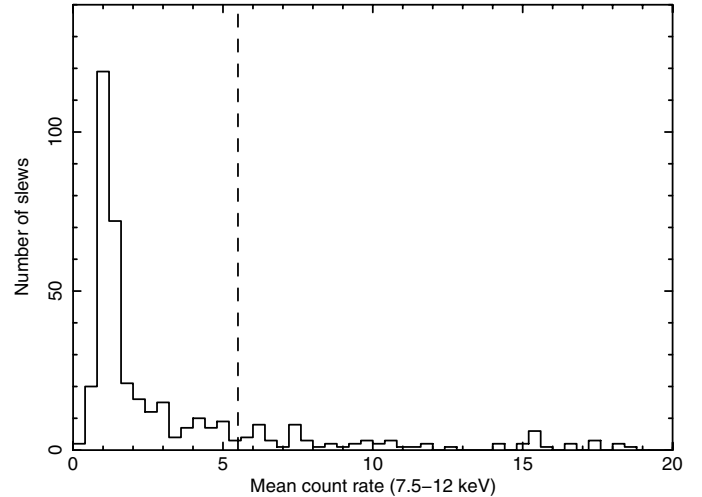

Fig. 1. The background level distribution measured from the mean 7.5–12 keV count rate in each slew. The dashed line shows the cut-off used to exclude high background slews in the tail of the distribution.

prime CCD. In the fast modes, *Timing* and *Burst*, only 1-dimensional spatial information for the central CCD is available and thus these modes are not well suited for source detection. It was discovered in initial tests that slews with a high background gave a large number of false detections and resulted in extremely long execution times for the source searching software. For this reason, slews with an average 7.5–12 keV (FLAG=0, PATTERN=0–4) count rate in excess of 5.5 c/s (25% of all slews), were excluded from the analysis (Fig. 1). This leaves a nominal 312 slews potentially useful for scientific analysis. In practice a significant number of slews were not able to be processed for a variety of reasons including failure to create exposure maps, unreasonably high exposure times, attitude reconstruction problems, missing keywords and the processing producing too large images. While it is strongly hoped that some of these datasets may be recoverable in the future by improvements to the processing system, for the purposes of this first catalogue they have been left out and the catalogue constructed from 218 slews. A list of the observation numbers of these slews is available at http://xmm.esac.esa.int/external/xmm_science/slew_survey/obsid_tab.html and the slew paths are shown in Fig. 2. About 4% of the covered area has been slewed over more than once and eventually a deeper survey will be available by combining overlapping slew data, especially near the ecliptic poles.

The EPIC-pn detector passes over a source in about 14 s depending on the position of the source and the angle subtended by the *Y*-axis of the detector to the slew path (the impact angle). Normally this is close to zero, but an impact angle of up to 20 degrees is possible. If the source passes through the detector optical-axis an effective on-axis exposure time of ∼11 s is achieved. In Fig. 3 we show the exposure time of the slew survey as a function of sky coverage. Due to the vignetting function, the mean exposure time is energy-dependent being 6.2 s in the soft (0.2–2 keV) band and 6.0 s in the hard (2–12 keV) band. Small ripples in the histogram are caused by gaps between the EPIC-pn CCDs and also by the different observing modes; in LW mode only half of the CCD is exposed and the maximum effective exposure time is 6 s.
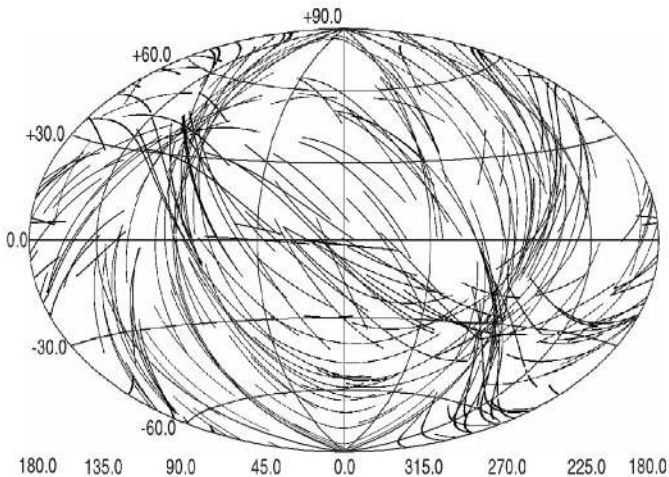
---

[1] The catalogue was initially released on May 3 2006. In this paper we discuss the updated version released in October 2006.
[2] This policy was changed from revolution 921 onwards to include all slews longer than 15 min.

Fig. 2. The paths of the slews used in the construction of XMMSL1 in Galactic coordinates.
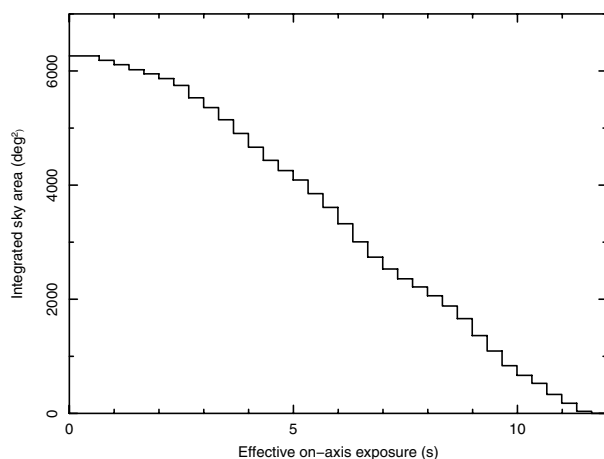

Fig. 3. A histogram of the cumulative sky area covered for a given effective on-axis exposure time in the total (0.2–12 keV) band.

3. Data processing

The data have been used to perform three independent surveys; a soft band (0.2–2 keV) X-ray survey with strong parallels to the ROSAT all-sky survey (Voges et al. 1999; RASS), a hard band (2–12 keV) survey and an XMM-*Newton* full-band (0.2–12 keV) survey.

Data reduction was performed as detailed below, with the public XMM-*Newton* Science Analysis Software (SAS), version 6.1 plus the following modifications:

- a modification for the `oal` library to handle the relatively large time gaps in the Raw Attitude File (RAF); subsequently released with `SAS v7.0`;
- an increase in the maximum number of attitude points which may be used by `eexpmap`; released with `SAS v6.5`.

3.1. Initial reduction

The XMM-*Newton* Slew Data Files (SDFs) for EPIC-pn were processed using the `epchain` package of the SAS. For diagnostic reasons a few parameters were set to non-default values (e.g. events below 150 eV were kept).

3.2. Slew division

Photon events are recorded initially in RAW or detector coordinates and have to be transformed, using the satellite attitude history, into sky coordinates. The tangential plane geometry commonly used to define a coordinate grid for flat images is only valid for distances of 1–2 degrees from a reference position, usually placed at the centre of the image. To avoid this limitation, slew datasets have been divided into roughly one degree by half a degree event files and attitude corrected using the task `attcalc`. Images and exposure maps were then extracted from the event files using the tasks `evselect` and `eexpmap`. This procedure relies on the attitude history of the satellite being accurately known during the slew; a point which is addressed in Sect. 4. Software, based on SAS and ftools (http://heasarc.gsfc.nasa.gov/ftools; Blackburn 1995), to perform the procedure of dividing and attitude-correcting slew data has been made available via the XMM-*Newton* web-site[3].

The procedure has been repeated in three separate energy bands: full band (0.2–0.5 keV [pattern=0] + 0.5–12.0 keV [pattern=0–4]), soft band (0.2–0.5 keV [pattern=0] + 0.5–2.0 keV [pattern=0–4]), and hard band (2.0–12.0 keV [pattern=0–4]). During the data processing stage severe problems with the transfer and storage of files from long slews were encountered. To alleviate this, only exposure maps for the full energy band were produced. This leads to an approximation being needed for exposure times in the different energy bands which is addressed in Sect. 6.3.

3.3. Source searching

Pilot studies were performed to investigate the optimum processing and source-search strategies. Uneven (and heightened) slew exposure is observed at the end of some slews (the "closed-loop" phase) and images with an exposure time greater than 20 s have been removed to ensure the uniformity of the survey. We tested a number of source-searching techniques and found that the optimum strategy was the usage of a semi-standard "eboxdetect (local) + esplinemap + eboxdetect (map) + emldetect" method, tuned to ~zero background, and performed on a single image containing just the single events (pattern=0) in the 0.2–0.5 keV band, plus single and double events (pattern=0–4) in the 0.5–12.0 keV band. This is similar to the technique used for producing the RASS catalogue (Cruddace et al. 1988) and resulted in the largest numbers of detected sources, whilst minimising the number of spurious sources due to detector anomalies (usually caused by non-single, very soft (<0.5 keV) events). The source density was found to be ≈0.5 sources per square degree to an emldetect detection likelihood threshold (DET_ML) of 10 (~3.9σ).

4. Attitude reconstruction and positional accuracy

The good point spread function of the X-ray telescopes (Aschenbach et al. 2000) should allow slew source positions to be determined to an accuracy of around 4 arcsec, similar to that found for faint objects in the 1XMM catalogue of serendipitous sources detected in pointed observations[4]. Any errors in the attitude reconstruction for the slew could seriously degrade this

---

[3] http://xmm.esac.esa.int/sas
[4] The First XMM-Newton Serendipitous Source Catalogue, XMM-Newton Survey Science Centre (SSC), 2003.

performance and a major technical challenge of the data processing has been to achieve the nominal accuracy.

The attitude information of the XMM-Newton satellite is provided by the Attitude and Orbit Control Subsystem (AOCS). A star tracker co-aligned with the telescopes allows up to a maximum of five stars to be continuously tracked giving accurate star position data every 0.5 s, which operates in addition to the Sun sensor that provides a precise Sun-line determination. Such information is processed resulting in an absolute accuracy of the reconstructed astrometry of typically 1 arcsec (1 sigma) for pointed observations. For the open-loop slews, large slews outside the star-tracker field of view of 3×4 degrees, the on-board software generates a three axis momentum reference profile and a two-axis (roll and pitch) Sun-sensor profile, both based on the ground slew telecommanding. During slew manoeuvring a momentum correction is superimposed onto the reference momentum profile and, as there are no absolute measurements for the yaw axis, a residual yaw attitude error exists at the end of each slew that may be corrected in the final closed-loop slew (Elfving 1999).

Two types of attitude data may be used as the primary source of spacecraft positioning during event file processing. They are the Raw Attitude File (RAF) and the Attitude History File (AHF). For pointed observations, the RAF provides the attitude information at the maximum possible rate, with one entry every 0.5 s while the AHF is a smoothed and filtered version of the RAF, with times rounded to the nearest second. In slew datasets the RAF stores attitude information every 40–60 s while the AHF contains the same records as the RAF with identical positions and again with timing information in integer seconds. The user can select which one to use for data processing by setting an environment variable.

In a pilot study where the AHF was used for attitude reconstruction, source detection was performed and correlations with the ROSAT and 2MASS catalogues indicated a slew relative pointing accuracy of ~10 arcsec. However, an absolute accuracy of 0–60 arcsec (30 arcsec mean) was obtained in the slew direction, resulting in a thin, slew-oriented error ellipse around each source. This error appears to be consistent with the error introduced by the quantisation of the time to 1 s in the attitude file and led us to change the processing software as a better accuracy should be obtained. As a test, the RAF was used to compute the astrometry for some observations. Here, an offset of ~1 arcmin from the ROSAT positions was found, but with a smaller scatter compared with the positions returned by the AHF processing. The consistency of these offsets suggested that they could be due to a timing issue. After discussions with the flight dynamics group it was realised that the star tracker CCD integration time of 0.75 s is not included in the times in the attitude history. When this 0.75 s is subtracted from every entry in the RAF we obtain an optimal attitude file for the processing. Note that this offset remains in all XMM raw attitude files but an automatic correction has been applied in the SAS software from version 7 onwards. Also note that this discrepancy has no practical effect on normal stable-pointed observational data.

Other issues affecting the astrometry performance appeared after a careful visual examination of the RAF files, where two types of peculiarities appeared in some of the slews affecting either a localised region or the totality of the slew. Five of the slews presented sharp discontinuities in the attitude reconstruction, revealing the existence of single bad RAF point. As an example a source in the slew 9073300002 was discovered to have a closest ROSAT counterpart at a distance of 8 arcmin. Investigation showed that the source was observed at a time coincident with
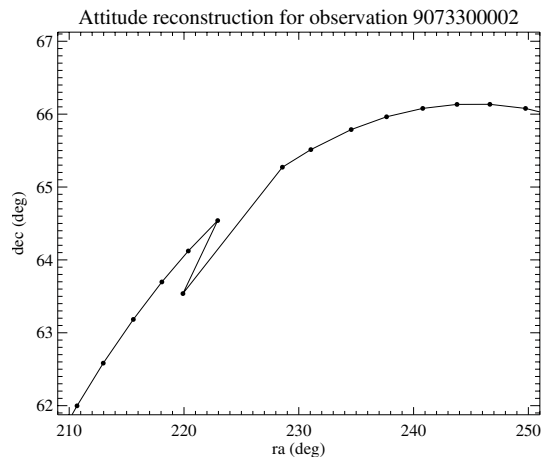

Fig. 4. A zoom into the problematic region of the attitude file in the slew 9073300002. The points show the generated attitude information.

a large error in the attitude file (Fig. 4). A test involving the removal of the bad point and recalculation of the attitude, while showing an improvement in source positions didn't improve the astrometry to the level of the other slews. Therefore, sources falling in a region of bad attitude have been flagged in the catalogue with the "Position Suspect" flag (see Sect. 5.1). Sections of seven other slews displayed an attitude reconstruction that can best be described as turbulent (Fig. 5). Again, sources falling in these slew sections have been marked with the "Position Suspect" flag.

A subsample of 1260 non-extended sources (defined as having an extent parameter <2 from the emldetect source fitting) with DET_ML > 10, have been correlated with several catalogues within a 60 arcsec offset. The correlation with the RASS reveals that 63% of the slew sources have an X-ray counterpart of which 68% (90%) lie within 16 (31) arcsec (Fig. 6). This gives confidence that the majority of slews have well reconstructed attitude. To form a sample of catalogues with highly accurate positions but which minimise the number of false matches, we used the Astronomical Virtual Observatory (AVO) to correlate the slew positions against non-X ray SIMBAD catalogues. This gave 508 matches of which 68% (90%) were contained within 8 (17) arcsec (Fig. 7).

5. The catalogue

Source lists were produced by searching each slew down to a likelihood DET_ML > 8 and combined to produce an initial catalogue of 5180 detections. This is available as the "full" catalogue where known spurious detections have been flagged out according to a set of criteria laid out in the next section.

5.1. Causes of spurious detections

5.1.1. Multiple detections of an extended source

The source detection software attempts to parameterise source extents up to 20 pixels (82 arcsec here) in radius. Larger sources, or sources with discontinuous or lumpy emission are reported as multiple small sources. This is particularly evident for the bright supernovae remnants (SNR), e.g. Puppis-A which results in 81 separate, confused, detections (Fig. 8). All affected sources have the VER_INEXT flag set true.
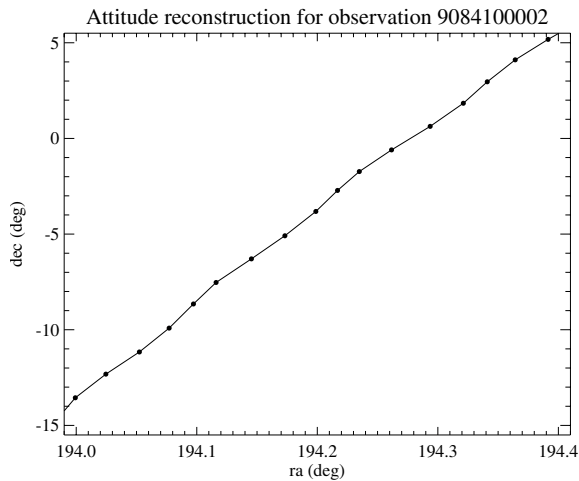
Fig. 5. A plot showing non-smooth, or turbulent, attitude reconstruction in the revolution 0841 attitude file.

5.1.2. The wings of the PSF of a bright source

It was noticed during the construction of the 1XMM serendipitous source catalogue that, due to the imperfect modelling of the PSF, a halo of false detections is often seen around bright sources. The same effect is seen in slew exposures but due to the reduced exposure time is only important for very bright sources ≫10 c/s. All affected sources have the VER_HALO flag set true.

5.1.3. High background

Flares in the background, due to solar protons (Lumb et al. 2002; Carter & Read 2007), cause a sudden increase in the number of events seen in a slew which mimic the effect of slewing over an SNR (Fig. 9). These flares typically last between 10 and 40 s and hence affect between 15 arcmin and 1 degree of a slew. No automatic flare screening has been performed on the data but light curves of all slews have been manually inspected and 175 sources, falling within flare-affected sections have been flagged as bad. All affected sources have the VER_HIBGND flag set true.

5.1.4. Bright sources outside detector field-of-view

Reflections from the CRAB SNR, about 10 arcmin outside the EPIC-pn field-of-view during the slew 9041000004, and the TYCHO SNR, 5 arcmin outside the field-of-view during the slew 9058600002, caused 5 false detections; VER_HALO flag set true.

5.1.5. Bad position

Seven sources are found near the edge of the detector or the edge of an image which leaves an uncertainty as to the true count rate of the source and where its centre lies. These sources have the VER_NREDG flag set true and also the VER_PSUSP flag set true to indicate that the position is suspect. In addition, sources in sections of slew with bad attitude (see Sect. 4) have their VER_PSUSP flag set true.

5.1.6. Zero exposure

Two sources are flagged as false because they lie at the very edge of the slew and are reported as having zero exposure time in one
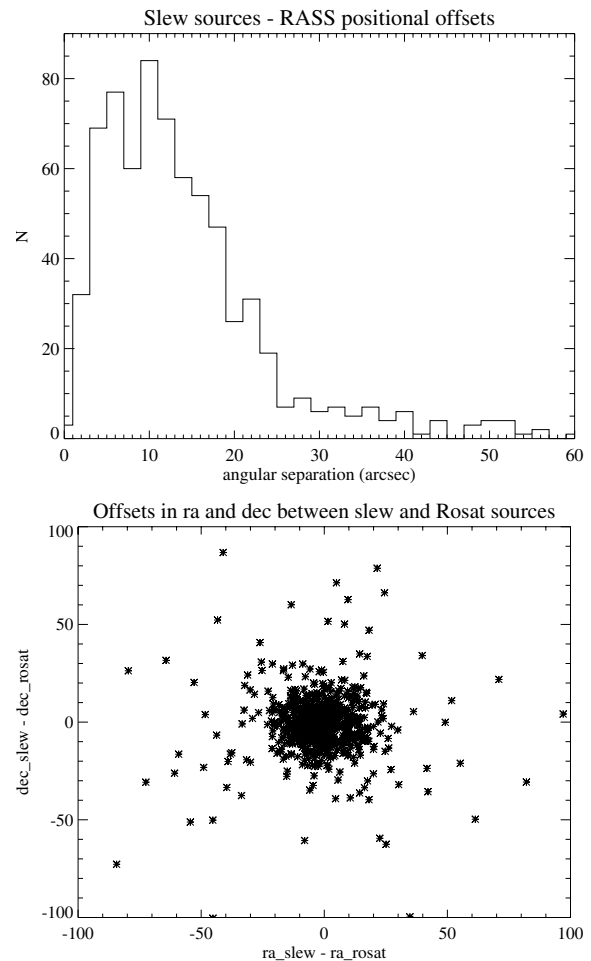

Fig. 6. A comparison of slew source positions with those from the RASS catalogue; 68% of the sources lie within 16 arcsec. The *upper panel* shows a histogram of the offset magnitude while the *lower panel* gives the absolute offset in arcseconds of the slew source from the ROSAT position.

or more of the energy bands. These have the VER_FALSE flag set true.

5.1.7. Optical loading

Despite initial concerns that the lack of a detector offset map during slews, would lead to optical loading problems, in practice little or no effect was found. In Fig. 10 we show a first magnitude star which is brilliant in raw slew data but completely disappears when the default event filtering is applied. None of the source fluxes in the slew catalogue are believed to be contaminated by optical photons.

5.2. Statistical fluctuations

The number of detections, after removing the spurious sources highlighted in the previous section, rises steeply with decreasing detection likelihood (Fig. 11) as expected. They are also seen to have a dependency on the background rate within the image in which the source was found (Fig. 12); where the background is defined as the event count rate above 10 keV ($PI > 10\,000$).

Simulations have been conducted to investigate the relationship between the number of spurious sources expected from background fluctuations and the number of events in an image.
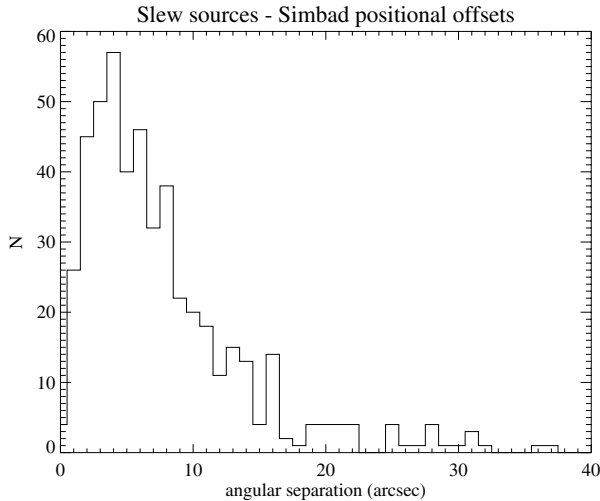
Fig. 7. A histogram of the distribution of the angular separation of the slew sources from their Simbad counterpart; 68% of the matches lie within 8 arcsec.
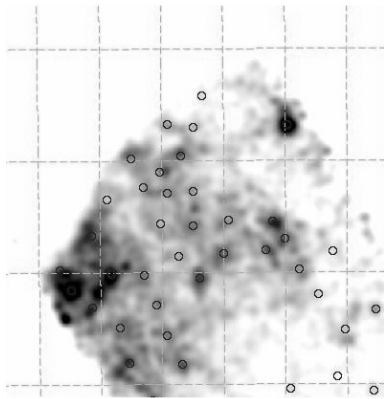

Fig. 8. The slew image of the large SNR, Puppis-A. It is detected as many small sources (circles).
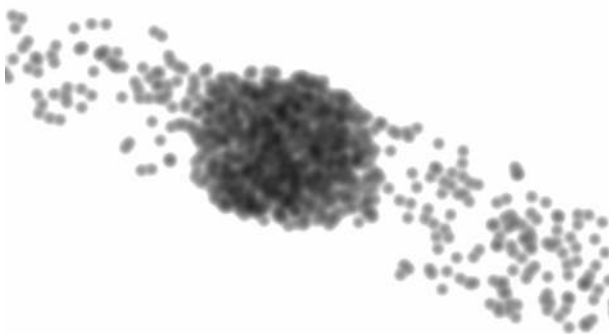

Fig. 9. A heavily smoothed section of the slew 9097100002. The bright patch of events in the centre has been produced by a background flare.

Simulated slew images have been created by inserting events into a template slew image, of 842 by 600 pixels and area 0.5 square degrees, at random positions. A flat spatial distribution of events has been used because the background is likely dominated by charged particle induced events, which show little variation across the detector, and internal flourescent emission
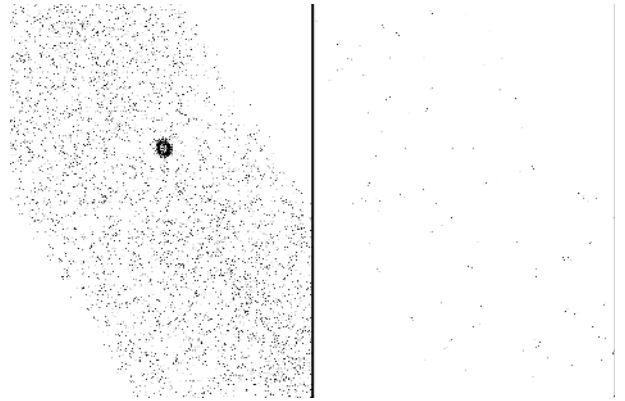
Fig. 10. *Left*: a raw image of gamma Cru, an M star with $m_v = 1.6$, detected in slew 90130900002. *Right*: the same image after applying the filter (FLAG==0, PATTERN==0, $PI > 200$).
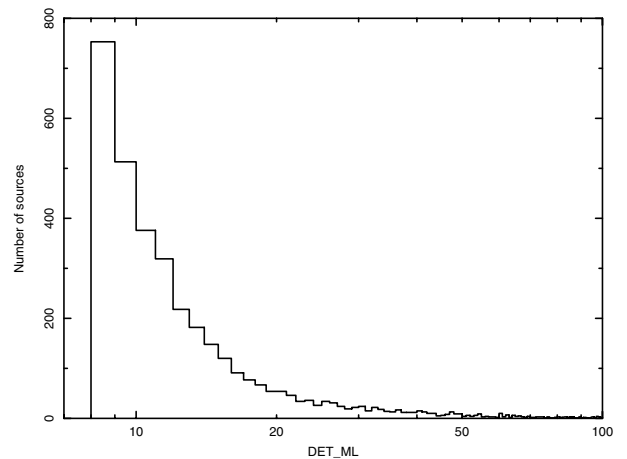

Fig. 11. Number of detections as a function of detection likelihood (total band; 0.2–12 keV).

lines which map the distribution of metals in the detector itself (Lumb et al. 2002). The resultant simulated images have been source searched and reveal a strong increase in the number of spurious detections with image counts, that rises steeply until around 500 events and then flattens out (Fig. 13). We have overlaid the distribution of counts in the real slew images in Fig. 13 to show that the majority of real images should generate few spurious sources for DET_ML > 12.

To assess the absolute number of false sources found by the source detection chain as a function of DET_ML, the positions of the photons in all 11137 slew images have been randomised and the images source-searched again. Results show that a significant number of sources with low DET_ML can be expected to be false. From Fig. 13 we know that the false source rate is influenced by the number of events in the image which is in turn related to the background rate. Selections of DET_ML and image background rate can be made from the simulation results to choose a particular spurious source fraction for a given purpose (Table 3). It is clear that the hard band, having typically a higher background than the soft band and a lower signal to noise ratio than either the soft or total band, is most affected by statistical fluctuations. A source selection [DET_ML > 14 or (DET_ML > 10 and image_bckgnd_rate<=3.0)] gives an expected 25 false detections from 259 hard band sources (~9%),
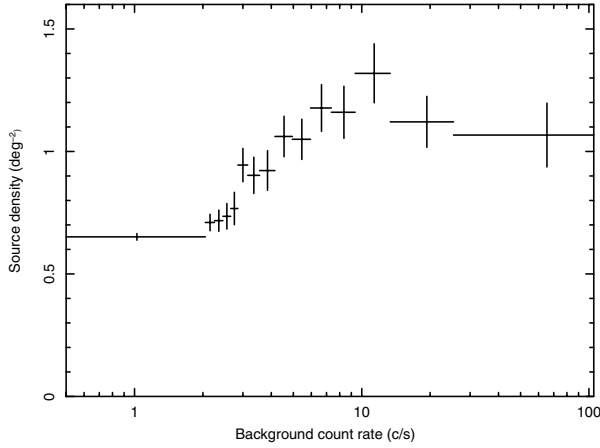
Fig. 12. The mean density of total band (0.2–12 keV) sources, flagged good in the full catalogue, plotted as a function of the background count rate ($PI > 10\,000$).
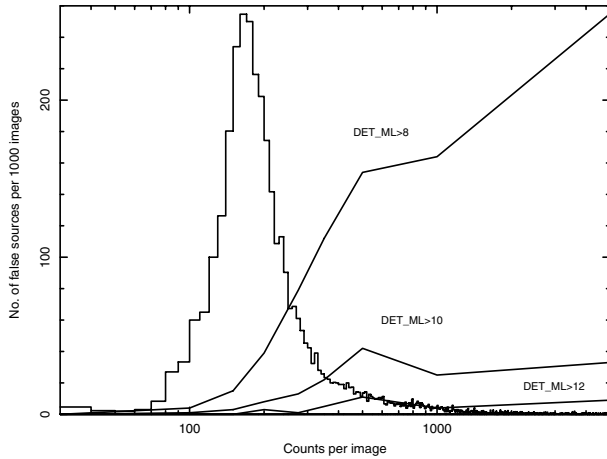

Fig. 13. The false source rate as determined from simulations. The histogram represents the distribution of counts in the real slew images.

13 from 1877 (0.7%) for the soft band and 109 from 2696 (4%) for all sources. Note that 80% of images have a background rate <= 3.0 c/s. A list of sources has been produced from this selection and is termed the "clean" catalogue. Finally, four sources which showed large position errors, due to the attitude file problems discussed in Sect. 4 had their VER_PSUSP flag set true in the "full" catalogue and were removed from the "clean" catalogue. This leaves a total of 2692 sources (257 in the hard band) in the "clean" catalogue.

5.3. Released catalogues

Both the "full" catalogue, with 5180 detections with DET_ML > 8 and the "clean" catalogue, with 2692 sources having DET_ML > 14 or (DET_ML > 10 and image_bckgnd_rate<=3.0) and the VER_INEXT, VER_HIBGND, VER_HALO and VER_FALSE flags set false (see Sect. 5.1) are available from http://xmm.esac. esa.int/external/xmm_data_acc/xsa. The catalogues contain columns with the detection threshold, background rate and spurious source flags sufficient to allow the user to select

Table 3. The number of sources found in slew images and in simulated slew images for combinations of minimum detection likelihood and background count rate.

ML[a]	bkg[b]	Band[c]			
	c/s	Combined	Total	Hard	Soft
8	–	4710/929	3863/580	692/272	2606/186
8	3.0	3451/456	3018/348	427/93	1981/69
10	–	2998/195	2580/118	312/61	2031/46
10	3.0	2419/106	2155/86	239/24	1638/13
12	–	2161/40	1875/28	185/12	1661/10
12	3.0	1782/21	1587/20	157/5	1354/2
14	–	1700/9	1470/7	139/4	1361/1
14	3.0	1423/6	1257/4	119/3	1122/1
10/14[d]	3.0/–	2696/109	2368/89	259/25	1877/13

[a] The minimum source likelihood.
[b] The maximum background rate accepted within an image, defined as the count rate of events with energy greater than 10 keV ($PI > 10\,000$).
[c] The number of detected sources (first number) and the number of expected false sources (second number) from simulations, in this energy band, for this combination of minimum detection likelihood and maximum background count rate. The "combined" band is made from the unique distinct sources detected in any of the total, soft or hard bands.
[d] A selection of all sources with DET_ML > 14 and sources with DET_ML > 10 from images where the background count rate is less than 3 c/s.

a subsample for a particular scientific purpose. The "clean" catalogue is conservative for the soft band but may not be strict enough for some applications in the hard band.

From hereon we discuss the properties of sources drawn from the "clean" catalogue unless otherwise stated.

6. Source properties

6.1. Naming convention

The adopted name for sources detected in the XMM-Newton slew survey starts with the prefix, XMMSL1, and then encodes the J2000 sky position, e.g. XMMSL1 J010537.6 + 364858. The name is assigned in two passes. When the three independent energy band source lists are combined to form one catalogue the source name is set using the position in the band where the DET_ML likelihood is the highest. A second pass is then performed such that sources which have been observed in more than one slew are given the same name. Again, priority is given depending on the detection likelihood. Detections are deemed to be from the same source if their centres lie within 30 arcsec of each other. Given the scarcity of slew sources (0.8 detections in the "full" catalogue per square degree) on the sky, 30 arcsec was found to be a reasonably robust match radius for point sources. It is not so good for extended sources and the catalogue in some cases contains multiple detections of the same extended source with different names.

6.2. Source extent

The source search algorithm attempts to parameterise detections as a point source or as an extended source with a radius of up to 20 pixels (82 arcsec). A large number of sources (30%) are detected as being extended (extension parameter > 1), The measured extension is related to the extension likelihood and to the number of source counts as shown in Fig. 14. Here it can be
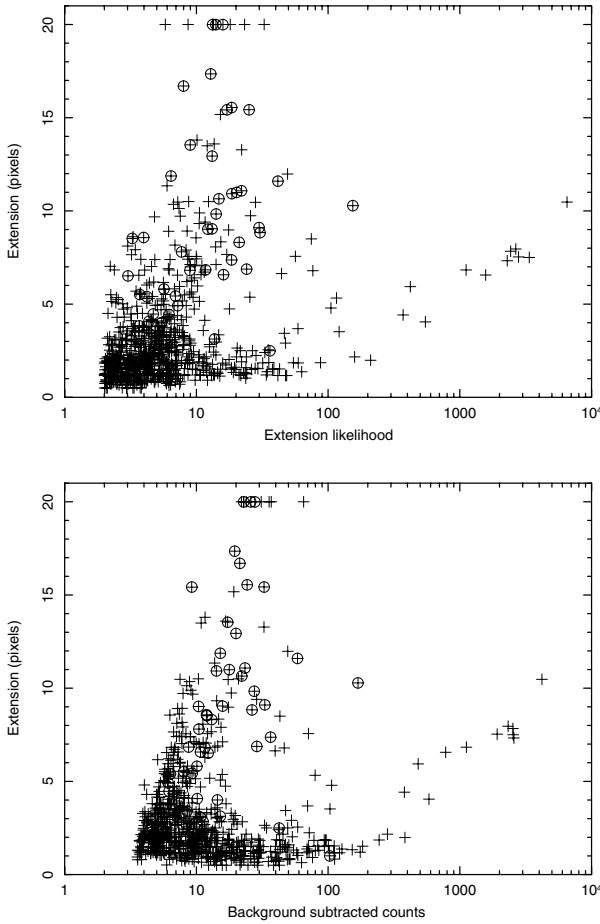
Fig. 14. Source extension, in units of 4.1 arcsec image pixels, plotted against the extension likelihood (*upper*) and number of source counts (*lower*) for extended sources detected in the total energy band. Sources identified as clusters of galaxies are marked with circles.

seen that there is an upper branch where an increasing number of photons are needed to detect larger source extensions and a lower branch where small extensions are found for a large range of source strengths and extension likelihoods. The point spread function (PSF) for the EPIC-pn detector is a function of off-axis angle (the distance between the optical-axis and the source). In the data analysis we have used the average off-axis angle of the path of a source through the detector, to calculate the appropriate PSF. This is reasonably accurate for the LW and FF modes where the frame time is short and the extension of the PSF along the slew direction small, but introduces an inaccuracy for the ~20% of observations taken in eFF mode, where the extension along the slew direction is ~18″ (Table 4). The lower branch is contaminated by false detections of extension caused by this effect which can be demonstrated by the fraction of eFF sources in this branch (35%) compared with the expected 20% in the upper branch. At large count rates, photon pile-up depresses the counts in the central pixels of the source profile also causing an apparent extension. A correct treatment of the slew PSF is needed to properly parameterise source extension, nevertheless sources falling in the upper branch of Fig. 14 are considered to be genuinely extended.

Table 4. Observing mode statistics.

Mode	Frame Time (ms)	Extension[a] (arcsec)	Fraction[b] %
FF	73	6.6	69
eFF	199	17.9	21
LW	48	4.3	10

[a] The extension of the PSF along the slew direction caused by the satellite movement during CCD integration.
[b] The percentage of the slew sky area covered in this mode.

6.3. Count rates

The count rates are calculated from the background subtracted counts within a circle about the source, corrected for the encircled energy fraction and divided by the PSF-weighted exposure time within the source region (see the *emldetect* user guide for more details [5]). For reasons of limited resources, source searching was performed in all bands using the exposure map for the total energy band. This produces incorrect exposures in the soft and hard bands due to the energy-dependent vignetting. A correcting factor:

$$e_h = 0.0013806 \times e_t^3 + 0.0085632 \times e_t^2 + 0.84282 \times e_t \tag{1}$$

$$e_s = 0.0014723 \times e_t^3 - 0.058884 \times e_t^2 + 1.3509 \times e_t \tag{2}$$

where e_s, e_h and e_t are the soft, hard and total band exposure times respectively, has been applied to the exposure times to correct for this effect. These factors were calculated by comparing several sets of total, soft and hard-band exposure maps and fitting a function to the relationship between the bands. This introduces a systematic uncertainty of ~5% into the soft and hard band exposure times and count rates. Due to the limit of 82 arcsec on source extent used by the search algorithm, sources extended beyond this value will have their count rate underestimated. Very bright sources are affected by photon pile-up which tends to reduce the count rate. The source strength limits for the observing modes are given by Strüder et al. (2001) for FF mode as 6 c/s and for LW mode as 9 c/s. For eFF mode the pile-up limit is in principle 2 c/s for a pointed observation but will be higher here as the slewing movement, together with the relatively long frame time, will reduce the count rate on the central pixel of the PSF.

A comparison of the soft band count rates against RASS count rates is presented in Fig. 15 for 894 non-extended sources with a ROSAT counterpart. The count rate ratio, XMM/RASS, is typically ~10 but varies considerably with the source spectrum. The comparison of these two surveys, coupled with upper-limits analysis represents a powerful tool for finding high variability X-ray sources. An initial analysis of high variability extragalactic sources found in this way has been published in Esquej et al. (2007).

6.4. Flux conversion

Source fluxes have been calculated from count rates based on energy conversion factors assuming a spectral model of an absorbed power-law with $N_H = 3 \times 10^{20}$ cm^{-2} and photon index 1.7 (see XMM science survey centre memo, SSC-LUX TN-0059, for a general description of the technique). The energy conversion factors are given in Table 5.
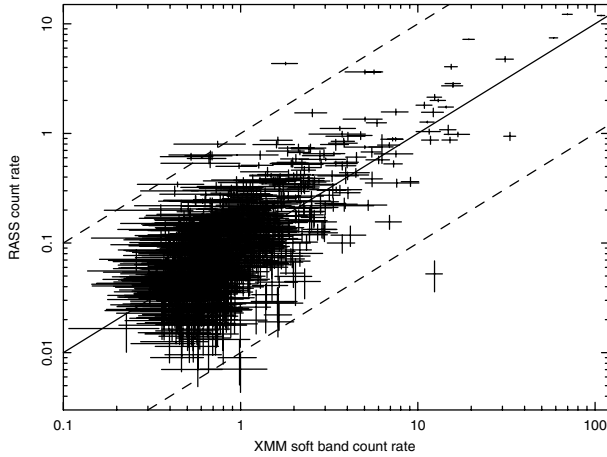
---

[5] http://xmm.esac.esa.int/sas/6.1.0/doc/emldetect/index.html

Fig. 15. A comparison of RASS and slew soft band count rates (c/s). The solid line represents a ratio of 10:1 and the dotted lines represent a factor of 10 variation from this value.

Table 5. Flux conversion factors.

Band	energy range (keV)	Conversion factor[a]
Total	0.2–12.0	3.16
Hard	2.0–12.0	9.14
Soft	0.2–2.0	1.44

[a] Converts from source count rate (c/s) to flux in the given energy band in units of 10^{-12} ergs/s/cm^2.

The soft-band fluxes are particularly dependent on the spectral model used and can be quite discrepant for stars where the absorbing column may be small.

At the fluxes probed here, source confusion within the 20 arcsec extraction radius is almost absent.

6.5. Hardness ratio

In Fig. 16 we plot the positions in Galactic coordinates of the soft and hard band sources and separately all the sources, colour-coded by hardness ratio. The hardness ratio is defined as

$$H_R = (S_H - S_S)/(S_H + S_S) \qquad (3)$$

where S_H is defined as the source count rate in the hard band and S_S as the count rate in the soft band.

As expected, hard sources, notably the bright LMXB, predominate in the Galactic plane and soft sources at higher Galactic latitudes.

6.6. Spectra

Spectral analysis of slew data is fundamentally complicated by the fact that a source bright enough to produce a reasonable spectrum will suffer from photon pile-up. A quantative analysis of these spectra awaits the implementation of a realistic pile-up correction and the development of an energy-dependent point spread function, which will be a vignetting-weighted average of the PSF at each detector position traversed by the motion of the source through the detector.
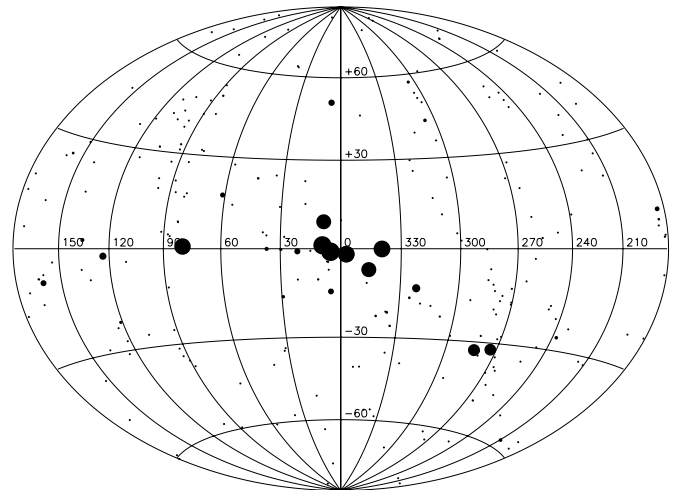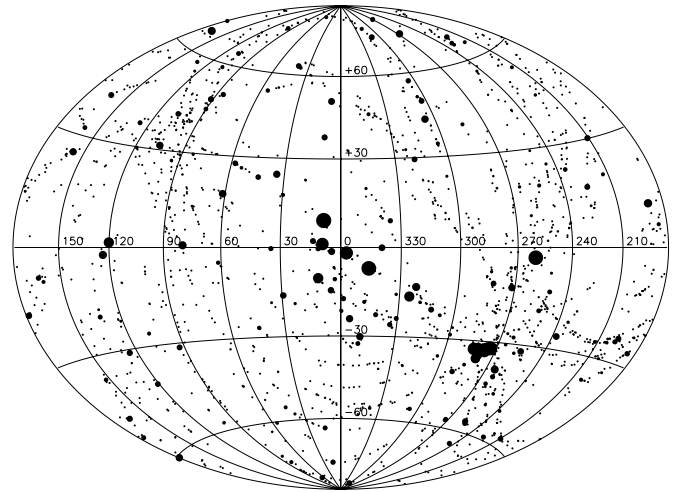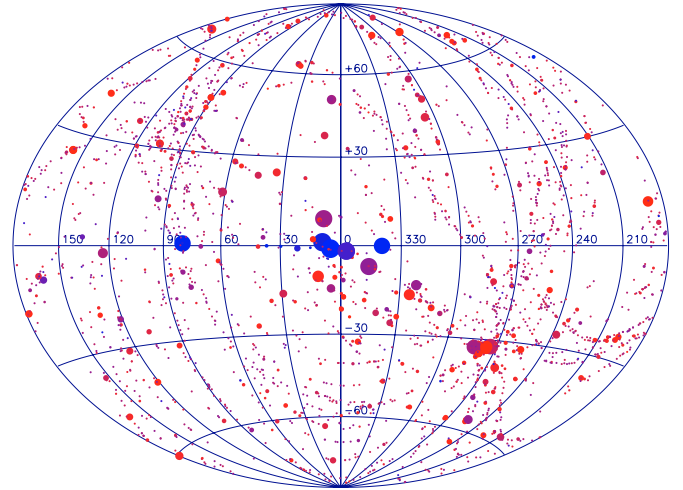

Fig. 16. An AITOFF projection in Galactic coordinates of sources from the first XMM-*Newton* slew survey, where the circle size scales logarithmically with the count rate. *Top panel*: the total band sources; the hardness ratio is colour-coded such that light red is soft and blue is hard. *Middle panel*: the soft band sources. *Bottom panel*: the hard band sources. The two bright sources seen in the hard-band plot at latitude ~−30 are LMC X-1 and LMC X-3.
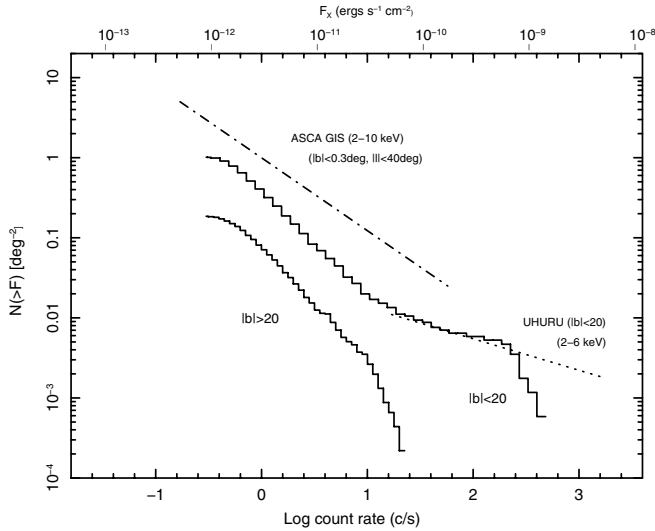
Fig. 17. The cumulative number count distribution of total band (0.2–12 keV) sources inside and outside the Galactic plane, plotted against count rate and absorbed flux. A spectral model of an absorbed power-law of photon index 1.7 and $N_H = 3 \times 10^{20}$ cm^{-2} has been used to convert the slew count rate into flux. The UHURU Galactic plane (dotted line; Forman et al. 1978) and the ASCA Galactic plane survey (dotdash line; Sugizaki et al. 2001) log N–log S relations have been displayed for comparison. In both of these cases the fluxes have been converted to an energy range 0.2–12 keV and to the above spectral model.

7. Sample properties

In Fig. 17 we show the cumulative number count distribution for the full energy band for sources within ($|b| \leq 20°$) and outside ($|b| > 20°$) the Galactic plane. A linear fit to sources outside the Galactic plane, in the central part of the distribution (log counts between –0.2 and 1.0) gives a slope of -1.41 ± 0.01. This is a little flatter than the Euclidian slope of 1.5 found by ASCA (Ueda et al. 1999) and earlier by HEAO-1 A2 (Piccinotti et al. 1982) and Ginga (Kondo et al. 1992). The difference in slope may be due to incompletenes, which appears to become evident in the source distribution below ~0.8 c/s. The distribution of sources within the Galactic plane shows a break at about 12 c/s ($F_{0.2-12} = 3.6 \times 10^{-11}$ ergs s^{-1} cm^{-2} for an absorbed power-law with $N_H = 3 \times 10^{20}$ cm^{-2} and photon index 1.7). At fainter fluxes the slope is -1.29 ± 0.02 while for brighter sources it is -0.43 ± 0.02. The bright source population agrees well with the previous result of UHURU (Forman et al. 1978), except at fluxes above $F_{0.2-12} \sim 8 \times 10^{-10}$ ergs s^{-1} cm^{-2} where gross pile-up effects significantly reduce the observed count rate (see Sect. 6.3). The log N–log S relation below $F_{0.2-12} = 3.6 \times 10^{-11}$ is steeper than the 0.79 ± 0.07 observed by ASCA in a survey with $|b| < 0.3°$ in the 2–10 keV band (Sugizaki et al. 2001). It is likely that the difference is at least partly due to the sky regions sampled. The wider XMM-*Newton* slew sample will, for example, contain a higher fraction of extragalactic sources. A thorough analysis of the log N-log S relation will require a careful analysis of the effects of pile-up, completeness, sky coverage and the Eddington bias and we defer this to a later date when a larger fraction of the sky has been covered.

8. Duplicate detections and variability

In the full catalogue 96 sources have been detected in more than one slew. Count rate variability up to a factor 5, 5 and 2 is seen in the total, soft and hard bands respectively. The greatest variability is seen in the total and soft band fluxes of XMMSL1 J125616.0-114632 (2MASXJ12561595-1146367); which varied by a factor 5 between slews 9037400004 and 9083600004 (a baseline of 2.5 years). An upper limits analysis will likely find greater variability.

9. Identifications

All sources detected in the survey have been correlated with different catalogues in order to identify the XMM-Newton slew sources with previously known objects (See Table 6 for a summary of the resources used). The catalogues used for this aim comprise two astronomical databases, a catalogue of clusters of galaxies and nine other catalogues (some which have been queried through the HEASARC astronomical database). Although the astrometric uncertainty of the slew sources was found to be 8 arcsec, the offset radius for the correlations was 30 arcsec (with a few exceptions described below) in order to include sources from catalogues with worse accuracy or truncated coordinates. For the EXOSAT CMA catalogue the offset radius was 45 arcsec, and for the Einstein IPC it was 2 arcmin, both due to the larger uncertainty in source coordinates. A radius of 5 arcmin was chosen for the clusters catalogue due to the extension of this type of object. The identification process results in unidentified sources, sources with a single counterpart and sources with multiple matches. A hierarchical selection scheme has been applied for sources with different counterparts. A decision has been made to derive the most plausible identification candidate using the technique described below. Firstly, the SIMBAD and NED astronomical databases have been used for the cross-correlation and results from both databases have been compared in detail (SIMBAD has been queried in the frame of the Astronomical Virtual Observatory (AVO)). When a source has the same counterpart in both databases the one selected for the identification is that which gives more specification about the source category. When contradictory identification candidates have been found, the one with the smallest positional offset has been chosen. These two databases provide the large majority (90%) of the total number of identifications. Then, a correlation with a clusters table (Abell and Zwicky Clusters of Galaxies) has been performed. The final identification for sources with a reported extension greater than 2 pixels, which have a SIMBAD/NED and also a cluster counterpart, comes from the clusters table. The remaining catalogues used for the cross-match are listed below ordered in priority for the preferred identification. For sources with multiple matches in a catalogue, the identification was selected as the closest match. These catalogues are: All-Sky Optical Catalog of Radio/X-Ray Sources, Catalog of PSPC WGA Sources, Einstein IPC Sources Catalog, EXOSAT CMA Images/Lightcurves, ROSAT All-Sky Survey catalogue, ROSAT Results Archive Sources for the PSPC, ROSAT Results Archive Sources for the HRI, RXTE Master Catalog, XMM-Newton Serendipitous Source Catalog, Version 1.1.0, INTEGRAL Bright Source Catalog. Results from

Table 6. Catalogues used for source identification.

Catalogue	match radius (arcsec)	Reference
SIMBAD	30	CDS[a]
NED	30	NED[b]
Abell clusters	300	Abell (1958)
Zwicky clusters	300	Zwicky et al. (1974)
All-Sky Optical Catalog of Radio/X-Ray Sources	30	Flesch et al. (2004)
Catalog of PSPC WGA sources	30	White et al. (1994)
Einstein IPC	120	Harris et al. (1994)
EXOSAT CMA	45	HEASARC[c]
RASS	30	Voges et al. (1999)
ROSAT PSPC Results Archive	30	HEASARC[c]
ROSAT HRI Results Archive	30	HEASARC[c]
RXTE Master Catalog	30	HEASARC[c]
1XMM V1.1.0	30	Watson et al. (2003)
INTEGRAL BSC	30	HEASARC[c]

[a] CDS, Strasbourg (2006).
[b] The NASA/IPAC Extragalactic Database (NED) is operated by the Jet Propulsion Laboratory, California Institute of Technology, under contract with the National Aeronautics and Space Administration.
[c] Data obtained from the High Energy Astrophysics Science Archive Research Center (HEASARC), provided by NASA's Goddard Space Flight Center.

the identification process appear in the final catalogue in the columns:

IDENT: name of the source

ALTIDENT: alternative name of the source

ID_DIST: distance in arcminutes between the slew source and the identification. Distances have been rounded to the nearest 0.1 arcmin to ensure a uniform accuracy across the catalogues.

ID_CATEGORY: type of the identified source that, when existing, has been extracted from the catalogues (it is not very homogeneous because type convention differs between catalogues)

RASSNAME: the closest RASS match

RASSDIST: distance in arcseconds to the closest RASS match.

Of the full catalogue sources, not flagged as spurious, 51% are identified. The fraction rises to 71% when only sources from the CLEAN catalogue are considered. Of these, 48% are extragalactic, 30% are galactic and the remainder are of unknown type, e.g. "X-ray source".

The identification list is expected to improve as more catalogues come on-line and with follow-up observations. The list is maintained at http://xmm.esac.esa.int/external/xmm_science/slew_survey/ident_tab.html and suggestions for counterparts are welcomed.

In Fig. 18 we plot the ratio of the X-ray to optical flux against the optical magnitude. Here we define the X-ray to optical flux ratio using the total band X-ray flux and the optical blue-band flux. Optical fluxes have been obtained either from the Simbad counterpart or from the USNO B1 magnitude for the cases where a single plausible match is found within the slew error circle. Distinct source types lie in distinct regions of the plane and
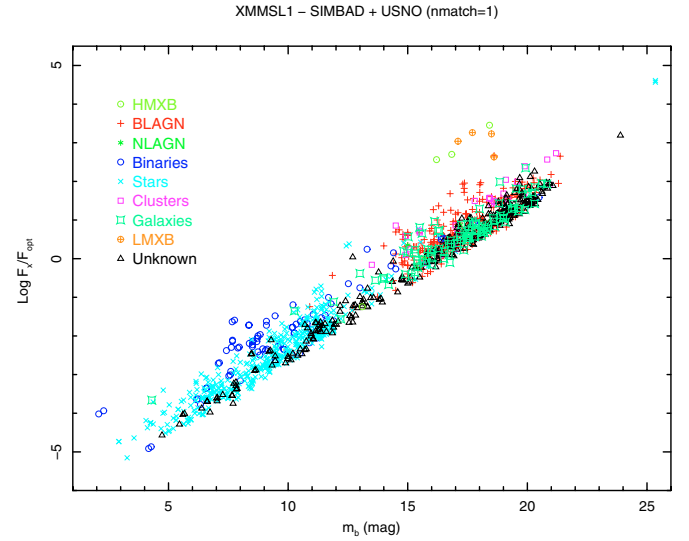

Fig. 18. The log of the ratio of the X-ray to optical flux plotted against the optical magnitude of the counterpart.

statistically it can be seen that the unknown sources with an unambiguous optical counterpart predominantly fall in the region occupied by AGN but there are also a significant fraction of sources which lie in the region occupied by stars and binaries that have not been assigned a source category.

Source types may be further distinguished by considering the X-ray hardness ratio (HR; e.g. Della Ceca et al. 2004). In general the low number of counts precludes an accurate measurement of the HR for slew sources. In Fig. 19 we show sources which have either a detection in the hard band or ≥ 10 counts in the soft band and use an upper limit of three photons in the case of a non-detection in one of the bands. The two points with the highest X-ray to optical ratio are two detections of the isolated neutron star RXJ 1856.6-3754. Unidentified sources are present in both the hard and soft regions of the plot.

10. Summary

The XMM-*Newton* slew data represent the deepest near all-sky hard band X-ray survey made to date, while the soft band survey is comparable with the RASS. The source density, from the clean catalogue, is ~0.45 per square degree and ~70% have plausible identifications. The XMM-*Newton* slew survey catalogue will continue to grow as the mission continues and it is expected that a sky coverage in excess of 50% will eventually be achieved. With the excellent attitude reconstruction this will leave a powerful legacy for future variability studies in the soft and hard X-ray bands.
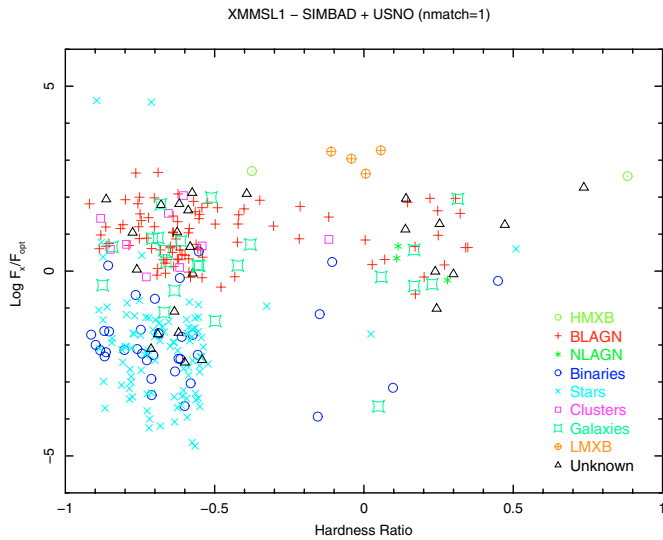
Fig. 19. The ratio of X to optical fluxes plotted against the X-ray hardness ratio. In the case of a non-detection in the hard or soft band, the hardness ratio has been calculated by assuming an upper limit of three photons in the non-detection band. For reasons of simplicity neither error-bars nor upper limit arrows are shown on the plot.

References

Abell, G. O. 1958, ApJS, 3, 211
Aschenbach, B., Briel, U. G., Haberl, F., et al. 2000, Imaging performance of the xmm-newton X-ray telescopes, in X-Ray Optics, Instruments, and Missions III, ed. J. Truemper, & B. Aschenbach, Proc. SPIE, 4012, 731

Blackburn, J. K. 1995, in Astronomical Data Analysis Software and Systems IV, ed. R. A. Shaw, H. E. Payne, & J. J. E. Hayes (San Francisco: ASP), ASP Conf. Ser., 77, 367
Brandt, W. N., Hornschemeier, A. E., Garmire, G. P., et al. 2000, AAS, 196, 3416
Carter, J. A., & Read, A. M. 2007, A&A, 464, 1155
Cruddace, R., Hasinger, G., & Schmitt, J. 1988, The application of a maximum likelihood analysis to detection of sources in the rosat data base, in Astronomy from Large Databases. Scientific objectives and methodological approaches, ed. F. Murtagh, & A. Heck, ESO Conf. and Workshop Proc., 177
Della Ceca, R., Maccacaro, T., Caccianiga, A., et al. 2004, A&A, 428, 383
Elfving, A. 1999, in ESA Bull., 100
Elvis, M., Plummer, D., Schachter, J., & Fabbiano, G. 1992, ApJS, 80, 257
Esquej, P., Saxton, R. D., Freyberg, M. J., et al. 2007, A&A, 462, L49
Flesch, E., & Hardcastle, M. J. 2004, A&A, 427, 387
Forman, W., Jones, C., Julien, P., et al. 1978, ApJS, 38, 357
Freyberg, M. J., Altieri, B., Bermejo, D., et al. 2005, ESA-SP, 604
Hasinger, G., Altieri, B., Arnaud, M., et al. 2001, A&A, 365, L45
Harris, D. E., Forman, W., Gioia, I. M., et al. 1994, SAO HEAD CD-ROM Series I (Einstein), 18
Jansen, F., Lumb, D., Altieri, B., et al. 2001, A&A, 365, L1
Jones, L., & Lumb, D. 1998, Proceedings of the First XMM Workshop, ESTEC, Noordwijk, The Netherlands, ed. M. Dahlem, http://xmm.vilspa.esa.es/external/xmm_science/workshops/1st_workshop/ws1_papers.shtml
Kondo, H., Dotani, T., Inoue, H., et al. 1992, in Frontiers of X-ray Astronomy ed. Y. Tanaka, & K. Koyama (Tokyo: Universal Acad.), 665
Lumb, D. 1998, AN, 319, 146
Lumb, D. H., Warwick, R. S., Page, M., & De Luca, A. 2002, A&A, 389, 93
Piccinotti, G., Mushotzky, R. F., Boldt, E. A., et al. 1982, ApJ, 253, 485
Reynolds, A. P., Parmar, A. N., Hakala, P. J., et al. 1999, A&AS, 134, 287
Revnivtsev, M., Sazonov, S., Jahoda, K., & Gilfanov, M. 2004, A&A, 418, 927
Read, A., Saxton, R., Esquej, P., Freyberg, M., & Altieri, B. 2006, PASJ, 58, L47
Sugizaki, M., Mitsuda, K., Kaneda, H., et al. 2001, ApJS, 134, 77
Strüder, L., Briel, U., Dennerl, K., Hartmann, R., & Kendziorra, E. 2001, A&A, 365, L18
Turner, M. J. L., Abbey, A., Arnaud, M., Balasini, M., & Barbera, M. 2001, A&A, 365, L27
Ueda, Y., Takahashi, T., Inoue, H., et al. 1999, ApJ, 518, 656
Voges, W., Aschenbach, B., Boller, T., et al. 1999, A&A, 349, 389
Watson, M. G., Pye, J. P., Denby, M., et al. 2003, AN, 324, 89
White, N. E., Giommi, P., & Angelini, L. 1994, IAUC, 6100
Zwicky, F., Herzog, E., Wild, P., Karpowicz, M., & Kowal, C. T. 1961–68, Catalogue of galaxies and of clusters of galaxies, California Institute of Technology, Pasadena, 6 vols